Eur. Phys. J. D **6**, 211–220 (1999)

THE EUROPEAN PHYSICAL JOURNAL D

EDP Sciences

Simple determination of Na_2 scattering lengths using observed bound levels at the ground state asymptote

A. Crubellier[1], O. Dulieu[1], F. Masnou-Seeuws[1,a], M. Elbs[2], H. Knöckel[2], and E. Tiemann[2]

[1] Laboratoire Aimé Cotton, CNRS II, bât. 505, Campus d'Orsay, 91405 Orsay, France
[2] Institut für Quantenoptik, Universität Hannover, 30167 Hannover, Germany

Received: 28 September 1998 / Received in final form: 21 December 1998

Abstract. A simple model is developed to determine a scattering length from the experimental values of the energy of the last, least bound, vibrational levels of the ground state, either $^1\Sigma_g^+$ or $^3\Sigma_u^+$, of an alkali dimer. It is based on an extrapolation of the positions of the few outermost nodes of the bound vibrational wave functions towards the dissociation threshold. It uses the asymptotic part of the molecular potential only. The method is applied to recently measured levels at the asymptote $(3s + 3s)$ of Na_2. We obtain precise values for the two scattering lengths respectively associated to the dissociation limits $F_1 = F_2 = 1, F = 2$ (55.1±1.6 a_0) and $F_1 = F_2 = 1, F = 0$ (50.0±1.6 a_0); the first value corresponds to the $a_{1,-1}$ scattering length usually considered in cold collisions. The extrapolation procedure is also applied to Li_2, using existing experimental data.

PACS. 33.20.Kf Visible spectra – 32.80.Pj Optical cooling of atoms; trapping – 34.50.Pi State-to-state scattering analyses

1 Introduction

A quantitative description of Bose-condensed alkali vapors, recently observed for Rb [1], Na [2] and Li [3], requires the knowledge of accurate low-energy atom-atom collision data such as scattering lengths. The stability of a condensate is indeed controlled by the sign of the scattering length [4–6]. *A priori* calculation of these parameters is known to be a very difficult task, because they depend very strongly upon the interaction potentials [7,8], which cannot be computed with sufficient accuracy at short or intermediate internuclear distances. Therefore, the use of experimental results appears to be necessary.

There are different approaches to determine accurate scattering lengths from experimental data. One is based on the observation of minima in the intensities of photoassociation spectral lines, which can be related to the position of the nodes of the wave function describing the collision of two ultracold atoms. The data are extrapolated from small to zero collision energy. This has been applied to Rb [9,10], Li [11], Na [12] and Cs [13].

A second approach uses spectroscopic data of bound vibrational levels of the ground state (singlet or triplet) of the diatomic molecule to extract potentials as accurate as possible, to compute the phases of the last levels and to extrapolate them towards the dissociation limit. To be accurate, this extrapolation requires that the energy difference between the highest measured levels and the dissociation limit is as small as possible. Abraham *et al.* [14] and Tsai *et al.* [15] recently measured the last, least bound levels of Li_2 and Rb_2 respectively, by two-color photoassociation spectroscopy, and have obtained very accurate values for the scattering lengths. For Na_2 and K_2 there also exist spectroscopic data, but ending at a few wave numbers below the dissociation limits, leading to larger uncertainties in the extrapolation [16,17]. In some cases, the observation of shape resonances connected to the centrifugal barrier has allowed to improve the determination of scattering lengths [10,18]. Very recently, the observation of Feshbach resonances induced by a magnetic field has also provided scattering length values, either directly, through photoassociation spectroscopy [19], or indirectly, by measuring the number of atoms in a Bose-Einstein condensate [20].

We present here results of a new spectroscopic experiment to measure the energies of the last bound levels in the ground $X^1\Sigma_g^+$ potential curve of Na_2. We then describe the method which we developed to extract the scattering length starting from such spectroscopic information. Our approach is related to the accumulated phase method [9, 21], and, more generally, to quantum defect theories [22, 23] and to Milne's method [24,25]: we use indeed the fact that the inner part of the wave function changes its shape very little for energies close to the dissociation threshold. The method involves only the generally rather well known asymptotic part of the adiabatic molecular potential (atomic hyperfine structure, dispersion and, if

[a] e-mail: fmasnou@lancelot.lac.u-psud.fr

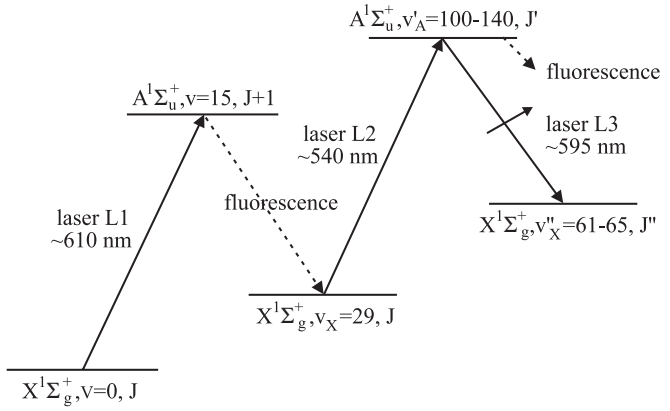

Fig. 1. Simplified experimental scheme to measure the last bound levels of $X^1\Sigma_g^+$.

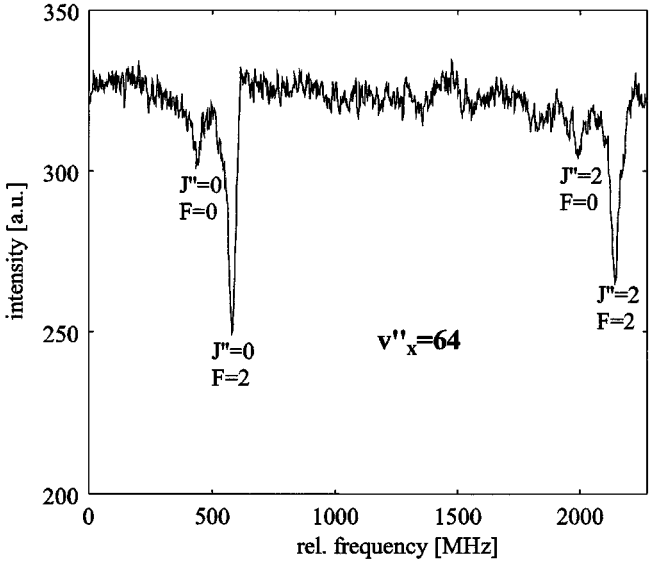

Fig. 2. Example for spectrum of asymptotic levels of $X^1\Sigma_g^+$. $\vec{F} = \vec{F}_1 + \vec{F}_2$ denotes the total angular momentum of the two atoms. The zero of the frequency scale is arbitrary.

necessary, exchange interaction). Its originality is to extrapolate towards the dissociation limit in a very intuitive way, based on the position of the outermost nodes in the vibrational wave functions, which provide an easy way to visualize the phase of the radial oscillation.

After a short description of the experiment (Sect. 2), we investigate the link between scattering length and node positions of the zero-energy s-wave scattering wave function (Sect. 3). In the next two sections, we describe the extrapolation procedure that we use to obtain, from the accurate spectroscopic data of Section 2, the positions of the outermost nodes of this zero-energy scattering wave function, which will in turn, using the results of Section 3, allow us to obtain the scattering length. In Section 4, we consider the simple case of a pure R^{-6} potential, which is also general since in such a model the different alkalis differ by a scaling factor only. In Section 5, a more precise Na_2 asymptotic potential is introduced in single channel calculations; the influence of channel coupling in the asymptotic region is then studied, to investigate the limitations of the single channel procedure.

2 Spectroscopy of the last bound levels of the $X^1\Sigma_g^+$ ground state of Na_2

For measurements of the last bound levels of $X^1\Sigma_g^+$ we extended the setup which we applied for the observation of asymptotic levels in the state $A^1\Sigma_u^+$ of Na_2 [26]. The principal scheme is described shortly here, details will be published elsewhere [27]. We start with a collimated beam of molecules, where mainly the few lowest vibrational levels (v_X=0, 1, 2) of $X^1\Sigma_g^+$ are populated. These levels cannot be connected to the last bound levels ($v_X > 60$) with a single Raman-type transition, neither using levels of the $A^1\Sigma_u^+$ state nor of the $B^1\Pi_u$ state as intermediates, due to negligible Franck-Condon overlap. Therefore, we use two steps as shown in Figure 1: first we populate intermediate levels of $X^1\Sigma_g^+$ (*e.g.*, $v_X = 29$) by Franck-Condon pumping realized by laser L1. Starting from these levels, there is reasonable Franck-Condon overlap for the Raman transition ($v_X = 29$) − (v'_A = 100-140) − (v''_X = 61-65). For detection we observe the fluorescence when scanning laser L3, while laser L2 is kept on resonance with the transition ($v_X - v'_A$). The fluorescence decreases, when laser L3 gets in resonance with the transition ($v'_A - v''_X$), completing the Raman cycle. A recording is shown in Figure 2, where we observe the resonances ($v'_A = 120, J' = 1$) − ($v''_X = 64, J''$=0, 2), while laser L2 is on resonance with the transition (v_X = 29, $J = 0$) − ($v'_A = 120, J' = 1$). In this example each rotational line is split into a doublet due to hyperfine splitting of $v''_X = 64$. For the levels $v''_X = 61$ to 63 the hyperfine structure is smaller and was not resolved in our experiment.

With this scheme we observed the last bound levels of $X^1\Sigma_g^+$ $62 \le v''_X \le 65, J'' = 0$, which are used throughout this paper. The value for $v''_X = 61$ was derived from observed transitions with $J'' \neq 0$. Additionally, we obtained data for $J'' = 1, 2, 3$ and for some levels of the triplet ground state $a^3\Sigma_u^+$ (the levels $v''_X \le 62$, have been observed earlier by Fourier-transform spectroscopy for $J'' =$ 13, 15 [28]). The observed linewidths for $J'' = 0$ are about 20 MHz, which allows an excellent experimental accuracy. For absolute calibration of the frequencies of the lasers L2, L3 we used the iodine absorption spectrum (for $v''_X \le 63$), saturation spectroscopy on some calibrated iodine lines [29] (for $v''_X =$ 64, 65) or a lambda meter (for L2), leading to estimated uncertainties of about 10 MHz for each calibration step for $v''_X = 64, 65$. In order to give the level energies with respect to the dissociation limit, we used the photoassociation measurement of the energy difference between ($3s^2S_{1/2}(F_1$=1) + $3s^2S_{1/2}(F_2$=1)) and ($A^1\Sigma_u^+$, $v' = 165$, $J' = 1$), which is equal to 16954.8828(10)cm^{-1} [30]. The results are given in Table 1, together with experimental uncertainties, assuming the different calibration steps to be independent. For

Table 1. Energies of the last levels of $X^1\Sigma_g^+$ with $J'' = \ell = 0$. The zero of energy is set at the dissociation limit $3s^2S_{1/2}(F_1 = 1) + 3s^2S_{1/2}(F_2 = 1)$.

v''_X	energy E_v [cm^{-1}]
61	−8.9710(25)
62	−4.2932(25)
63	−1.6238(25)
64 ($F = 0$)	−0.3744(9)
64 ($F = 2$)	−0.3696(9)
65 ($F = 0$)	−0.0131(7)
65 ($F = 2$)	−0.0106(7)

$v''_X = 64, 65$ the uncertainty is dominated by the photoassociation step. The $v''_X = 65$ level is definitely the last vibrational level below the $F_1 = 1$, $F_2 = 1$ asymptote.

As the considered levels are very loosely bound, the wave function is mainly located in the asymptotic region, where the angular momentum $\vec{\ell}$ associated to the nuclear motion can be considered as decoupled from the total angular momentum $\vec{F} = \vec{F}_1 + \vec{F}_2$ of the two atoms. In the theoretical interpretation, we shall always use the symbol ℓ instead of the spectroscopic convention J''.

3 Nodes of threshold radial wave functions and scattering length

The radial Schrödinger equation for the relative radial motion of the atoms can be integrated either inwards or outwards: only the boundary conditions differ. Starting from the inner region, the same boundary condition holds for bound and free states: the wave function exponentially vanishes when the interatomic distance becomes shorter than the position of the repulsive potential wall at the considered energy. However, when the integration starts from the outer region, an exponential boundary condition still holds for bound states only. For free states corresponding to relative motion with energy E and angular momentum ℓ, the asymptotic behavior in the outwards region is controlled by the phase shift $\delta_\ell(E)$. For near threshold wave function with small positive energy E and $\ell = 0$ angular momentum (s-wave), and in the case of a single potential $V(R)$[1], the phase shift is simply related to the scattering length L, defined by

$$L = \lim_{K\to 0}\left[-\frac{1}{K}\tan(\delta_0(K))\right], \tag{1}$$

where

$$E = \frac{\hbar^2K^2}{2\mu}, \tag{2}$$

and μ is the reduced mass. The behavior at large interatomic distance R is thus completely determined by the scattering length L. Starting from infinite R, one has to solve the equation

$$\left(\frac{\hbar^2}{2\mu}\frac{\mathrm{d}^2}{\mathrm{d}R^2} - V(R) + E\right) f(R) = 0, \tag{3}$$

where $f(R)$ is proportional to $\sin(K(R-L))$ for $R \to \infty$. Using this boundary condition, the wave function at any distance can be readily obtained by inward integration. As we are interested neither in the inner part of the wave function, nor in its normalization, we can stop the integration before the actual potential $V(R)$ diverges from its asymptotic form, having nevertheless already obtained the positions of the outermost nodes. For the sake of simplicity, we at first restrict the potential to a $-C_6/R^6$ term, which is the leading long-range interaction term for the ground state of alkali dimers: equation (3) reduces then to a quite general form:

$$\left(\frac{\mathrm{d}^2}{\mathrm{d}x^2} + \frac{1}{x^6} + k^2\right) y(x) = 0, \tag{4}$$

where lengths are divided by the scaling factor

$$\alpha = \left(\frac{2\mu C_6}{\hbar^2}\right)^{1/4}, \tag{5}$$

which depends upon the reduced mass μ and the asymptotic coefficient C_6, and where wave numbers are multiplied by the same factor:

$$k = K\alpha. \tag{6}$$

For the threshold wave function ($k = 0$), the boundary conditions can be set:

$$\begin{aligned} y(x) &= -1 + x/l, \\ y'(x) &= 1/l, \end{aligned} \tag{7}$$

where we have introduced a reduced scattering length, $l = L/\alpha$. (Note the difference between l, the normalized scattering length, and ℓ, the quantum number of the angular momentum.) Equation (4) is easily solved numerically by inward integration (we used "Mathematica" software, which employs a Runge-Kutta procedure), providing in a straightforward manner the positions of the last nodes x_n of the threshold wave function which corresponds to any arbitrary value of the scattering length.

It is also possible, for $k = 0$, to solve equation (4) analytically (see [31,7]) and to get an analytical relation between the position x_n of the n-th node of $f(x)$ (for any n value) and the reduced scattering length l; this is in fact possible for any x^{-p} potential, with $p > 3$ and one has generally:

$$l = \frac{\Gamma\left(\frac{p-3}{p-2}\right)}{(p-2)^{2/(p-2)}\Gamma\left(\frac{p-1}{p-2}\right)} \frac{J_{-\frac{1}{p-2}}\left(\frac{2}{(p-2)x_n^{(p-2)/2}}\right)}{J_{\frac{1}{p-2}}\left(\frac{2}{(p-2)x_n^{(p-2)/2}}\right)}, \tag{8}$$

[1] Provided it decays asymptotically faster than R^{-3}, see [31].

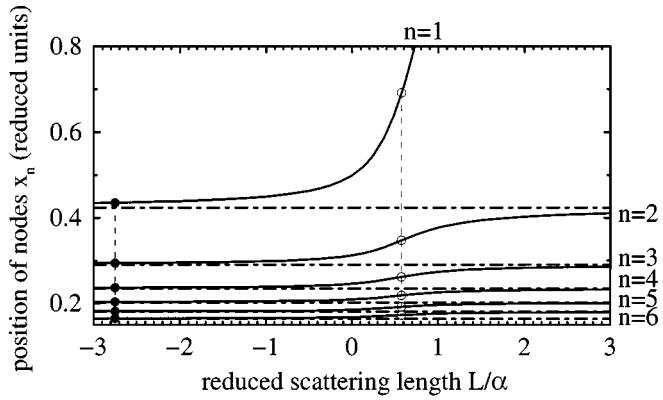

Fig. 3. Position (in reduced units) of the few outermost nodes of the $E = 0$, $\ell = 0$ (s-wave) scattering wave function *versus* reduced scattering length. The horizontal asymptotes (dashed-dotted lines) correspond to the node positions for (either positive or negative) infinite scattering length. The two thin vertical lines are drawn as examples of node positions of the wave function for two particular values, $l = -2.75$ and $l = 0.58$.

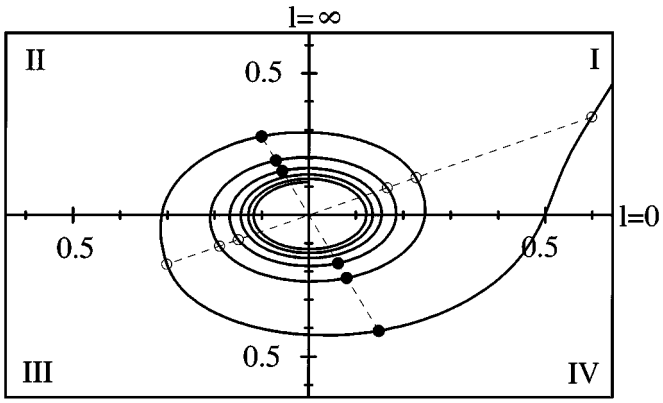

Fig. 4. Same as Figure 3, but in polar coordinates (r, θ). The radius r is node position, in reduced units, and the angle θ is related to the reduced scattering length by $l = \tan(\theta)$. The two broken lines show the node positions for the same two examples as in Figure 3, $l = -2.75$ ($\theta = -70°$) and $l = 0.58$ ($\theta = 30°$).

where J_m is a Bessel function with fractional order m [32].

Whatever the integration method, either numerical or analytical, it appears that there is a simple one-to-one correspondence (with analytical form given by equation (8)) between the scattering length and any node position of the threshold s-wave wave function. In other words, any x_n value is associated to a single l value. This is clearly manifested in Figure 3, where the positions of the first six nodes (counted from infinite x or R) of the threshold radial s-wave wave function, obtained by numerical inward integration, are displayed as a function of l. We have also drawn two vertical lines to show examples of sets of node positions for two values of the scattering length, one positive, the other negative. It is striking that the position of the outermost node, labelled $n = 1$, is the most sensitive to the l value, especially in the $l > 0$ region. One also notices that the limit of node positions for infinite positive l and infinite negative l is the same. This property becomes more obvious in Figure 4, where we have drawn a polar plot of the node positions *versus* the angle θ defined by

$$l = \tan(\theta)\,. \tag{9}$$

The determination of θ is chosen to ensure the continuity of the graph: quadrants I and III (respectively, II and IV) correspond to positive (respectively, negative) l values. When θ is increased around $\pi/2$, l changes from positive to negative values through infinity and the outermost node of quadrant I goes to infinity and disappears, whereas, as is well known, the last bound level disappears at the well top. Lines of nodes corresponding to the same l values as in Figure 3 are drawn for comparison. These results can be used to determine a scattering length from the position of a node of the s-wave function which can be deduced from the analysis of the intensities of vibrational progressions in photoassociation spectra (see, for instance, [9,13]). It will be shown below that it also allows us to determine a scattering length by using the positions of the least bound levels of the ground state (either $X^1\Sigma_g^+$ or $a^3\Sigma_u^+$).

The results shown in Figures 3 and 4, which correspond to a pure R^{-6} behavior of the potential, can be readily extended to potential curves with any asymptotic behavior (provided it decays faster than R^{-3}): the numerical procedure provides similar graphs but an analytic solution is available for pure R^{-p} potentials only.

4 Extrapolation of node positions of bound radial wave functions: pure R^{-6} potential

4.1 Last nodes of radial wave functions of bound states

Let us consider the last few outermost nodes of some weakly bound wave functions of a deep potential well. For any state, the phase accumulated from the innermost node up to the i-th node is equal to $(i-1)\pi$. Provided that the energy difference between the considered levels is small compared to the potential well depth, the phase accumulation will proceed, as R increases, almost identically for the different levels. The positions of the i-th nodes will thus be about the same for all considered levels. More precisely, the line connecting these positions as a function of level energy (which will be called here i-nodal line) is expected to decrease very slowly with increasing energy. The same argument holds for continuum states with small collision energy values. Finally, if we consider levels with binding energies small compared to the potential well depth, the positions of the i-th nodes can be safely extrapolated up to the $E = 0$ threshold and little beyond.

The asymptotic part of the least bound wave functions can be calculated by using the asymptotic potential only, provided the integration is started from infinite R. Such an integration can be performed for any energy, E, by solving the equation

$$\left(\frac{\mathrm{d}^2}{\mathrm{d}x^2} + \frac{1}{x^6} - k^2\right)\, y(x) = 0\,, \tag{10}$$

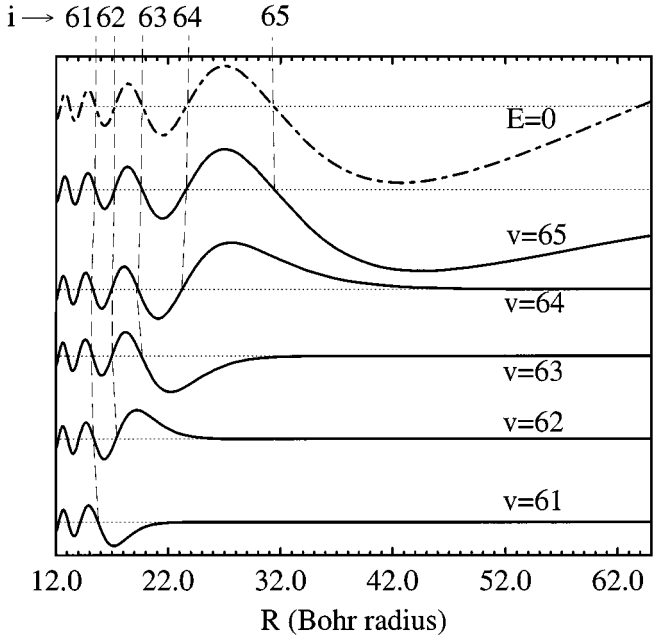

Fig. 5. Asymptotic part of the wave functions of the last five bound vibrational levels of Na_2 ground state (with $F_1 = F_2 = 1, F = 2$). The wave functions are not normalized; they are adjusted so that the inner part is about the same for all wave functions. The thin dashed lines join successive nodes with same i-number, for $i = 61$ to 65. The thick dashed-dotted line is the zero-energy scattering wave function with adjusted scattering length as obtained in Section 4.3.

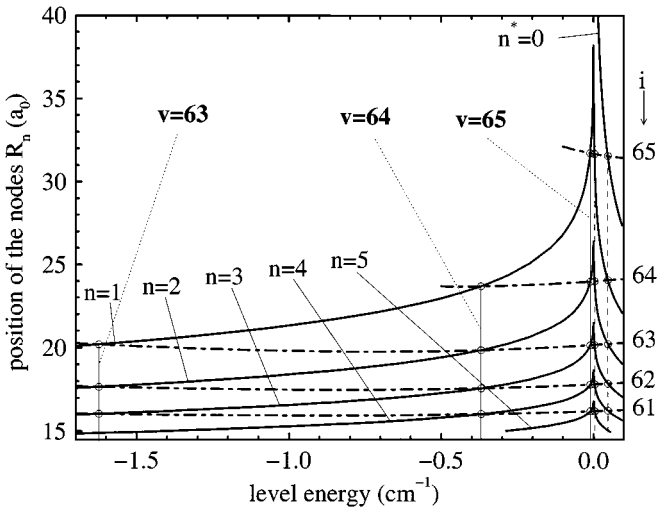

Fig. 6. Illustration of the extrapolation procedure. The x-axis represents energies with respect to the dissociation threshold (in cm^{-1}), the y-axis represents interatomic distances (in a_0) corresponding to nodes of radial wave functions. The calculation uses the adiabatic potential of Na_2 leading to the dissociation limit $F_1 = F_2 = 1, F = 2$ and the experimental energies of Table 1; the general shape is quite similar for any asymptotic potential with a R^{-6} leading term. We have drawn as thick solid lines: the first five n-nodal lines (see text) corresponding to bound states, their continuation for "virtual states" and the first additional nodal line of these states. Also drawn are the vertical lines at the experimental energy of vibrational levels $v = 63$ to 65 (thin solid lines) and at the predicted energies of the first two virtual states, E_c^1 and E_c^2 (thin dashed lines). Finally, the thick dot-dashed lines represent i-nodal lines (see text) whose number is indicated on the right. Node positions of the zero-energy s-wave scattering wave function are located at the intersection of the latter curves with the $E = 0$ axis.

with

$$E = -\frac{\hbar^2 k^2}{2\mu\alpha^2}\,, \tag{11}$$

and by using an exponential boundary condition.

We display in Figure 5 the result of such calculations for the five upper levels $v = 61$ to $v = 65$ of Na_2, using the experimental energies of Table 1 (we have chosen $F = 2$ for the two upper levels). The vibrational wave functions are drawn as a function of the internuclear distance R. From the vibrational labelling of the levels it is easy to identify the numbering of the nodes: according to the usual convention in which the nodes are numbered from small to large R values (i-numbering), the last node of a vibrational wave function v has a number $i = v$, the last but one $i = v - 1$, etc. We have drawn in the figure the broken lines joining the positions of the nodes with same number i (the i-nodal lines), with i varying from 61 to 64. It is clear that, as expected, these lines are almost straight and vertical. The considered energy range (about 9 cm^{-1} from $v = 61$ to $v = 65$) is indeed very small compared to the well depth of the potential (about 6022 cm^{-1}).

The thick solid lines of the region $E < 0$ of Figure 6 display the positions of the last few nodes of the wave functions obtained by inward integration of equation (10), as a function of E (the figure is not drawn in reduced coordinates, but in normal coordinates, in the Na_2 case, for $C_6 = 1539$ a.u. [33], $\mu = 20953.891$ a.u. and thus $\alpha = 89.61\ a_0$). Of course, as actual bound state wave functions are solutions of an eigenvalue problem, the computed wave functions have a physical meaning only if the chosen E value corresponds to an eigenvalue of the complete equation: this can be fulfilled, as done in Figure 5, by using the experimental results of Table 1 and by performing the integration choosing $E = E_v$, E_v being the energy with respect to the dissociation threshold of a level with vibrational quantum number v.

Nodes of vibrational bound states v can also be numbered from large to small distances (n-numbering). The relation between the two numbers of a given node is simply

$$i + n = v + 1\,. \tag{12}$$

The solid lines of Figure 6 correspond to n-numbering: we call them n-nodal lines to distinguish them from the i-nodal lines, which one would obtain by outward integration at any E value. The i-nodal lines can also be obtained by joining intersections of the n-nodal lines with verticals at the experimental energy values: in Figure 6 examples of i-nodal lines with $i = 63, 64$ and 65 are given. One sees that these lines are very smooth so that they can be safely

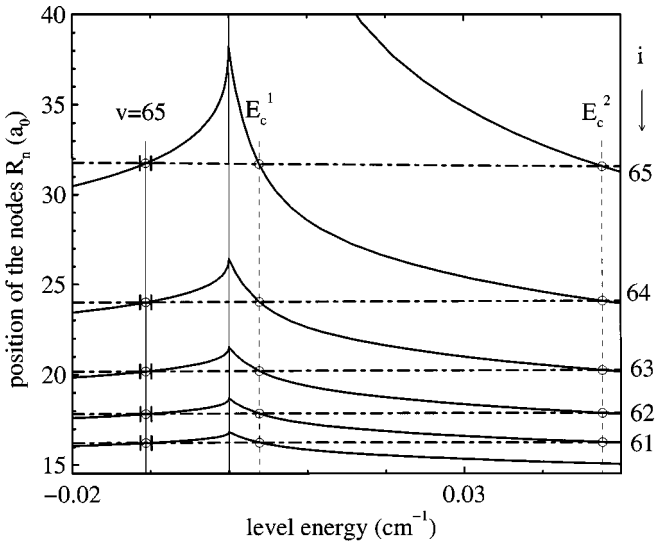

Fig. 7. Zoom of the $E = 0$ region of the preceding graph. The experimental uncertainty on the measured energy of the $v = 65$ vibrational level is indicated.

extrapolated to $E = 0$, giving the node positions of the threshold wave functions. From the results of Section 3, each i-nodal line will then yield one independent determination of the scattering length; the complete set will be used for internal consistency check.

4.2 Last nodes of radial wave functions of virtual states

In the continuum region, the states with phase shift equal to $\pi/2$, sometimes called virtual states, form a natural continuation of the bound state series: the wave functions of the first virtual states are expected to resemble much the ones of the last bound states, at least in the inner region. The node positions of these wave functions for any positive energy value can also be obtained by inward integration of equation (4) with boundary condition:

$$y(x) = \sin(kx - \pi/2)/\sqrt{k}\,. \tag{13}$$

The positions of some nodes of such continuum states (restricted to small E values and to the R range of the previously calculated n-nodal lines of bound states) are displayed as a function of E in Figure 6 (solid lines of the $E > 0$ region). Due to their oscillatory behavior, continuum states have an infinite number of nodes, which can be numbered from inwards but not from outwards. However, as can be seen in Figure 6, any n-nodal line corresponding to bound states is continued across $E = 0$ (but with discontinuous derivative[2]) by a nodal line of virtual states, which is thus called n^*-nodal line by continuation. Virtual states form additional n^*-nodal lines (one such line appears in Figure 6), which can be numbered $n^* = 0$, $n^* = -1$ etc. by simple continuation of the naming. Virtual states themselves can be labeled as $v^* = 66$, 67 etc. and equation (12) can finally be generalized to virtual states as $v^* = n^* + i$. The nodes of virtual states with given i-number form a natural extension of the i-nodal lines of the bound states. It will be shown hereafter that this extension is helpful in the extrapolation procedure, for increasing the internal consistency of the method.

4.3 Extrapolation procedure

Now the extrapolation procedure is almost evident. First, choose a series of experimental energy values E_v (in our case, v is running from 61 to 65) with $\ell = 0$ which correlate to a given dissociation limit, *i.e.* with a fixed set of atomic quantum numbers (in our case $F = 0$ or $F = 2$ for $3s^2S_{1/2}, F_1 = 1$ and $3s^2S_{1/2}, F_2 = 1$). Then, calculate the first few n-nodal lines for bound states and their analogs for virtual states; five lines ($n = 1$ to 5) corresponding to bound states and six lines ($n^* = 1$ to 5 and $n^* = 0$) corresponding to virtual states are represented by solid lines in Figure 6. Draw the vertical lines corresponding to all experimental E_v values (from $v = 61$ to $v = 65$, in our case): their intersection with the solid lines give the positions of the last nodes of the bound wave functions. Find then, from equation (12), their i-number. Use lowest order polynomial interpolation procedure (we have checked that the chosen interpolation method does not really matter; the experimental error on the measured energies will fully determine the uncertainty of the derived $E = 0$ node positions and thus of the scattering length) to connect the nodes with same i-number (dot-dashed lines of Figure 6). The i-nodal line with smallest i value (61 in our case) is almost a straight horizontal line and extrapolation can safely be used along this line to find the position E_c^1 of the first continuum state with $\pi/2$ phase shift. Draw now the vertical line (thin dashed) at E_c^1 to obtain the predicted positions of the nodes of the corresponding continuum wave function. Use again an interpolation procedure to connect all nodes with same i-number, belonging to either continuum or bound states (dot-dashed lines in Figure 7, which is an enlarged portion of the most interesting region of Figure 6). An additional i-line, involving the last node, $i = 65$, of the last bound state, $v = 65$, now appears. The extension to the continuum states introduces an additional constraint for the i-nodal lines, whose crossings with n-nodal lines must align vertically, not only in

[2] This discontinuity, obtained here for a potential that behaves asymptotically as R^{-6}, is specific to s-waves and does not appear for other ℓ values. The top of each cusp corresponds to a node position in case of infinite scattering length. Near threshold, an i-nodal line corresponding to large positive (respectively, negative) scattering length is close to a horizontal just below (respectively, above) a cusp point. Therefore one expects both a real and a virtual near-threshold state in the case of large positive scattering length, and neither a real nor a virtual near-threshold state in the case of large negative scattering length. This is very different from the usual case of finite-range potential, where a real (respectively, virtual) near-threshold state is predicted in case of large positive (respectively, negative) scattering length.

Table 2. Various determinations of the C_6 coefficient for Na-Na interaction with reference given in the first column. The last but one used a recently measured value of the sodium atom polarizability [38].

Ref.	C_6 (a.u.)
[34]	1540
[35]	1527
[36]	1472
[37]	1500
[33]	1539
[33]	1561

the $E < 0$ region (bound states) but also in the $E > 0$ region (virtual states). From the values of the interpolation functions at threshold we obtain the positions of the nodes of the $\ell = 0$ (s-wave) zero-energy scattering wave function[3]. Either from the results of Figures 3 and 4 or from equation (8), we finally find the scattering length values corresponding to these node positions.

4.4 Results

Using this procedure with the two sets of experimental energy levels for $F = 0$ and $F = 2$ of Table 1, we have determined the corresponding scattering lengths, that we note, respectively, L_S^0 and L_S^2. The five i-nodal lines yield the same value (with relative differences of the order of 0.01%), which clearly demonstrates the internal consistency of the extrapolation procedure. The final results depend on the scaling factor α defined by equation (5) (in Fig. 6, y-axis is proportional to α and x-axis to α^{-2}), *i.e.* on μ and C_6. Several recent determinations of the C_6 coefficient exist (see Tab. 2 and Refs. [34–37,33]). Among the various determinations, we have chosen the value 1539 a.u., recently computed by a model potential taking into account a new measured value of the atomic polarisability [38], which remains coherent with the C_8 and C_{10} values that we use [36]. The scattering length values that we obtained for two different values of C_6 are shown in Table 3 (in brackets). The uncertainty coming from the measurement of the energy of the vibrational levels is estimated to be 1.6 a_0. It is essentially determined by the error of the binding energy of the last level ($v = 65$) also shown as error bar in Figure 7. The energy difference between the $v = 64$ and $v = 65$ levels is indeed known with a better accuracy (0.0005 cm^{-1}) than the two binding energies, separately.

The values L_S^0 and L_S^2 corresponding to the two dissociation channels, $F = 0$ and $F = 2$, differ by 5 a_0 (about 10 %), which is larger than the experimental uncertainty. In addition, the accuracy of the difference between L_S^0 and L_S^2 is certainly still better than the one of the separated

[3] As n-nodal lines concern either bound or virtual states only, the nodes of the $E = 0$ wave function do not belong to any n-nodal line; their n-number is one unit larger than the n-number of the preceding node on the same i-nodal line.

Table 3. Computed values (in Bohr radius, a_0) of the scattering lengths with $F = 0$ and $F = 2$, using two different values of the C_6 coefficient, with references given in first column. The values in brackets correspond to a pure R^{-6} potential. The estimated uncertainty is $1.6a_0$.

Ref.	C_6 (a.u.)	$F_1 = F_2 = 1, F = 0$		$F_1 = F_2 = 1, F = 2$	
[36]	1472	49.95	(49.58)	54.99	(54.68)
[33]	1539	49.98	(49.64)	55.10	(54.80)

values, since the energy differences between the pairs of levels $F = 0$ and $F = 2$ for $v = 64$ and $v = 65$ have been directly measured with a great accuracy (0.0003 cm^{-1}).

The influence of the C_6 value in this determination appears to be very small, and is not readily given by the scaling factor α (Eq.(5)). A variation of C_6 by about 4% results in a variation of the scattering length of the order of 0.1% only, while α is varying by 1%. As we shall see in the next section, these conclusions still hold when using a more refined asymptotic potential.

As can be seen from the preceding results, the method has a good internal consistency. Its two basic assumptions are that the scattering is due to a unique potential and that the multipole expansion can be limited to a leading term, *e.g.*, R^{-6}. In the next section, we will try to estimate the role of other terms of the asymptotic potential and the influence of the channel coupling.

5 Influence of the shape of the asymptotic potential and channel coupling

5.1 Adiabatic potentials

We now consider more precise adiabatic asymptotic potential curves, by using the following procedure. We have calculated the matrix elements of the R^{-6}, R^{-8}, R^{-10} terms of the multipole expansion [36], of the hyperfine interaction and of the exchange energy (following the model of Ref. [39]) in a state basis written as

$$\left|\gamma\ 3s\ ^2S_{1/2} I\ F_1\ 3s\ ^2S_{1/2}\ I\ F_2\ FM\right\rangle_{s,a}\ , \qquad (14)$$

where $I = 3/2$ is the nuclear spin of a sodium atom and which is an either symmetrized or antisymmetrized two-atom wave function in which the total angular momenta F_1 and F_2 of each atom with electronic quantum numbers $3S_{1/2}$ are coupled into the total angular momentum F (excluding the rotation). All the matrices are easily obtained: the dispersion terms are proportional to the unity matrix, the hyperfine interaction is diagonal, with hyperfine splitting equal to 1771.6 MHz [40], and the calculation of the exchange energy only requires a simple recoupling (implying a $9j$-symbol) of angular momenta. The asymptotic adiabatic potentials obtained by diagonalization of the sum of these matrices are shown in Figure 8, choosing $C_6 = 1539 a.u.$ [33] and the data of reference [36] for C_8 and C_{10}. The figure is split into three parts, to show first

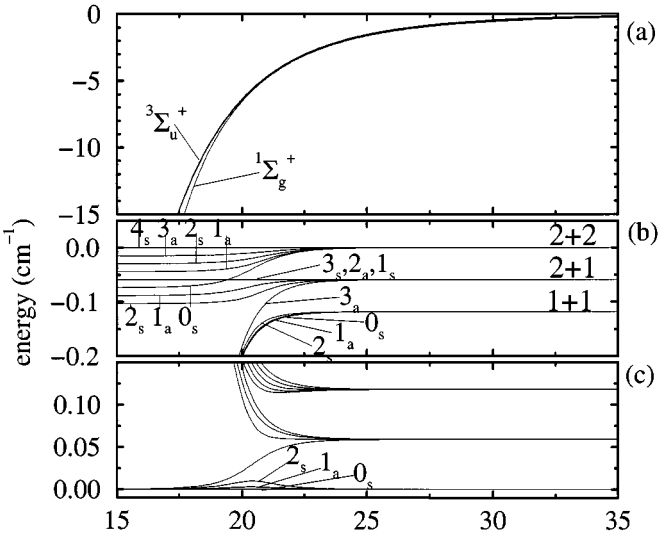

Fig. 8. (a) Asymptotic part of the adiabatic potential curves for the subspace of $a^3\Sigma_u^+$ and $X^1\Sigma_g^+$ states. (b) Same potentials as in (a), but the energy of the highest triplet curve was subtracted from all curves, to show the differences between the potentials with different F with either symmetric and antisymmetric electronic wave function. (c) Same as in (b), but the energy of the lowest symmetric potential with $F = 0$ was subtracted from all curves. The asymptotic quantum numbers are F_1 and F_2.

the general shape of the potentials (a), then the labels of all different adiabatic curves (b) and finally the energy difference between the two curves we are interested in (c).

We have calculated the two scattering lengths L_S^0 and L_S^2 accessible from the experimental data by the extrapolation procedure of Section 4, using now the two adiabatic curves corresponding, respectively, to $F_1 = F_2 = 1, F = 0$ and $F = 2$ instead of the pure R^{-6} potential. The results are shown in Table 3; they are essentially equal to those obtained by using a pure R^{-6} potential (Sect. 4). The uncertainty coming from the experiment is estimated to 1.6 a_0 and the whole discussion of Section 4.4 is still valid. The value L_S^2 found for the dissociation channel $F_1 = F_2 = 1,\ F = 2$, which is usually known as $a_{1,-1}$, is in good agreement with a previous determination $a_{1,-1} = 52 \pm 5\ a_0$ [12]. The latter was obtained by the NIST group from coupled channel calculations and fitting the observed intensity pattern in the photoassociation spectrum recorded for a cold Na ensemble. The value L_S^0 that we found for the other dissociation channel, $F_1 = F_2 = 1,\ F = 0$, is notably different from L_S^2, by about 10%, although both dissociation channels are connected to $X^1\Sigma_g^+$ states and although the two adiabatic curves are very close to each other (see Fig. 8, part (c)).

5.2 Channel coupling

The agreement of our scattering length value L_S^2 with previous determination using coupled channel calculations might be an indication for the validity of the single channel calculations that we performed. So does the fact that, for each set (either $F = 0$ or $F = 2$) of measured bound levels, the various i-nodal lines yield the same value for the scattering length. Conversely, the i-nodal lines drawn in Figure 6 are not monotonically decreasing, as one would expect for a series of vibrational eigenstates calculated in the single-channel picture. Additionally, we have checked that the small hump characterizing the difference between the asymptotic parts of the two adiabatic potentials (see Fig. 8 (c)) cannot be responsible for any appreciable phase shift. The difference between the two measured scattering length values has thus to be attributed to channel coupling. As, in the asymptotic region (see Fig. 8), all potentials are very close to each other, even small non-diagonal matrix elements of the radial coupling might lead to significant non-adiabatic effects.

To discuss these points more precisely, we consider the quantum-mechanical treatment of channel coupling in the asymptotic region. The coupled equations are written in a fixed frame and only radial coupling appears. We write the coupled solution as

$$\Phi_\beta(R;\mathbf{r}_i) = \sum_{\alpha=1,N} G_{\beta,a}(R)\Psi_\alpha(R;\mathbf{r}_i)\,, \qquad (15)$$

where the $G_{\beta,a}(R)$ are the radial components on the N coupled channels and the $\Psi_\alpha(R;\mathbf{r}_i)$ are the electronic wave functions associated to the adiabatic curves $V_\alpha(R)$. The radial wave functions are solutions of the system of N coupled equations:

$$\left(-\frac{\hbar^2}{2\mu}\frac{\mathrm{d}^2}{\mathrm{d}R^2} + V_\alpha(R) - E_\beta\right) G_{\beta,\alpha}(R) = \sum_{\alpha'\neq\alpha}\left(\frac{\hbar^2}{2\mu}\left\langle\Psi_\alpha\middle|\frac{\partial^2}{\partial R^2}\Psi_{\alpha'}\right\rangle + \frac{\hbar^2}{\mu}\left\langle\Psi_\alpha\middle|\frac{\partial}{\partial R}\Psi_{\alpha'}\right\rangle\frac{\partial}{\partial R}\right)G_{\beta,\alpha'}(R), \qquad (16)$$

where the notation $\langle\ |\ \rangle$ indicates the integration over the electronic variables. In the case we are interested in (see Fig. 8 (b)), one has three coupled equations for the (symmetrical) states with $F = 2$ (and any M value): ($F_1 = 2$, $F_2 = 2$), ($F_1 = 1$, $F_2 = 2$) and ($F_1 = 1$, $F_2 = 1$); one has two coupled equations for the (symmetrical) states with $F = 0$ and $M = 0$: ($F_1 = 2$, $F_2 = 2$) and ($F_1 = 1$, $F_2 = 1$). The values of the coupling terms in the asymptotic region are easily obtained from the eigenvectors characterizing the adiabatic curves. All of them are equal to zero everywhere except in a small range (from about 15 a_0 to about 27 a_0 in our case). However, most of the nodes that we consider (except for the last i-nodal line) are within the region where the coupling is not negligible.

A complete solution of the coupled equations for the last bound states is impossible in the asymptotic model without additional experimental information. For $N = 1$, the case of Section 4, we have an eigenvalue problem with two boundary conditions, one being located at the inner potential wall and being therefore unusable: we replace it by using the experimental energy as eigenvalue. For $N = 3$, one has an eigenvalue problem with six boundary conditions, three being unusable. Thus one would need

the eigenvalues corresponding to the 3 different $F = 2$ states forming the coupling space. It is, however, possible to compute some solutions of the coupled equations at the experimental energies. We have in particular computed by inward integration the coupled solution whose probability on the $F_1 = F_2 = 1$ channel is equal to one at infinite interatomic distance, for the energy values E_v with $v = 61$ to 65 and at $E = 0$. For the two coupled systems that we consider, the positions of the nodes that we obtain in this way do not differ from the ones obtained in the adiabatic picture by more than 1%. Taking into account the influence of channel coupling in the asymptotic region does not thus appreciably change the determination of the scattering length. Two effects combine to yield this result. Firstly, the channel coupling is weak in the asymptotic region. The last i-nodal line ($i = 65$) lies completely outside of the region of radial coupling and this is almost true for $i = 64$. Starting from these node positions, the determination of the $E = 0$ scattering wave function requires only the pure adiabatic potentials or, almost equivalently, the simple R^{-6} potential (this explains the small difference between the results that we obtained in the two models). Secondly, and this is probably the main strength of the model, the influence of channel coupling in the inner region is accounted for in the experimental energy values.

6 Conclusion

We have reported accurate spectroscopic measurements of vibrational levels at the asymptote $F_1 = F_2 = 1$ of the ground state of Na_2. The high resolution of the experiment (about 20 MHz) allowed us, for the highest v values (64 and 65), to resolve the hyperfine structure and to measure the difference between levels with two different values of the total angular momentum F, which correspond to two different dissociation channels. We have also shown that such spectroscopic measurements yield very accurate determination of the two corresponding scattering lengths.

The determination has been done here in a very simple and rather general way. We use only the asymptotic part of the potential curves and we perform straightforward numerical integrations, in contrast with other methods which deal with the whole potential and solve coupled equations. In its simplest form, which is already quite efficient, our model applies to the ground states, either $X^1\Sigma_g^+$ or $a^3\Sigma_u^+$, of any alkali dimer. The key point of the method is to characterize the phase of a wave function (of a continuum state as well as of a bound state) by the positions of its nodes, which are easy to compute and which allow simple graphic representations. In the considered case ($X^1\Sigma_g^+$ states), the results depend very little on the chosen asymptotic potential and the accuracy is directly related to the precision of binding energy measurements.

The value $L_S^2 = 55.1 \pm 1.6\ a_0$ found for the dissociation channel $F_1 = F_2 = 1,\ F = 2$, which is usually known as $a_{1,-1}$ when determined from scattering data, is in good agreement with elaborate calculations fitted on photoassociation spectra [12]. For the other dissociation channel for which experimental results were available, $F_1 = F_2 = 1,\ F = 0$, we found a value of $L_S^0 = 50.0 \pm 1.6\ a_0$, which differs from L_S^2 by about 10%. It is the first time, to our knowledge, that scattering lengths of two different dissociation channels which are both correlated to the singlet ground state can be compared directly, through independent measurements. The difference is important, although the two adiabatic curves are very close to each other (see Fig. 8). The origin of this difference cannot be found in the slight hump of $F = 2$ compared to $F = 0$ (see Fig. 8) and should thus be found in channel coupling. In any case, in view of this result, it appears that it would be very interesting to have experimental data corresponding to all other dissociation channels.

In order to further test our method, we did a determination of the scattering lengths of the triplet ground state of ^{6}Li and ^{7}Li, for which previous determinations existed. For ^{7}Li, we have used the measured energy values of the last vibrational level ($v = 10$) [41], and of the $v = 7$ one [42]; we find then a value of $-27.9 \pm 0.4\ a_0$; the value that the same authors obtained by adjusting the whole potential to all available experimental energies is $-27.3 \pm 0.8\ a_0$ (later revised as $-27.6 \pm 0.5\ a_0$ in [14]). In the case of ^{6}Li, Abraham *et al.* in reference [14] found a scattering length of $-2160 \pm 250\ a_0$ by using in particular a direct measurement of the binding energy of the highest-lying bound state. Using this energy (which corresponds to $v = 9$), together with the binding energy of the level $v = 7$ [42], we too find a large negative value of the scattering length (with an absolute value of a few thousands). The uncertainty is, however, very large, not only because of the lack of a measured value of the $v = 8$ level, but especially because, for large scattering length values, small variations in the node positions give huge variations of the scattering length (see Fig. 3).

It is worth mentioning that, once the scattering length is known, it is possible to use reciprocally our model to predict, at least roughly, the position of the last bound levels. We did it for the triplet ground state of Na_2, using the determination of reference [12], $a_{2,-2} = 85 \pm 3\ a_0$. The corresponding predicted level energies with respect to the $F_1 = 2 + F_2 = 2$ asymptote (0.1182 cm^{-1} above $F_1 = 1 + F_2 = 1$) are, for $\ell = 0$, $F = 4$ and for the last three v values: $E_v = -0.003$ cm^{-1}, $E_{v-1} = -0.15$ cm^{-1} and $E_{v-2} = -0.85$ cm^{-1}. There is no coupling to other potentials because $F = 4$ is a single channel. From new observations of the triplet state [27] with the method described in Section 2, the assignment of these predicted levels to absolute vibrational quantum numbers is straightforward; $v = 15$ is the last vibrational level of this triplet potential.

In conclusion, we have proposed a very simple and intuitive method to connect the energies of the last bound levels to the scattering length. We derive the scattering length from the asymptotic part of the $E = 0$, $\ell = 0$ threshold wave function, which is extremely close to the wave function of the last bound level. As we calculate the latter by using its experimental energy position, we account for channel coupling in some effective way: this is

probably the reason why the method can compete favorably with elaborate close-coupling calculations.

The work at Hannover was supported by the Deutsche Forschungsgemeinschaft within the SFB 407.

References

1. M.H. Anderson, J.R. Ensher, M.R. Matthews, C.E. Wiemann, E.A. Cornell, Science **269**, 198 (1995).
2. K.B. Davis, M.-O. Mewes, M.R. Andrews, N.J. van Druten, D.S. Durfee, D.M. Kurn, W. Ketterle, Phys. Rev. Lett. **75**, 3969 (1995).
3. C.C. Bradley, C.A. Sackett, J.J. Tollett, R.G. Hulet, Phys. Rev. Lett. **75**, 1687 (1995).
4. L. Landau, L. Lifchitz, *Physique Statistique*, chapt. VII, par. 78 (Mir, Moscow 1967).
5. E.P. Gross, Nuovo Cimento **20**, 454 (1961).
6. L.P. Pitaevski, Sov. Phys. JETP **13**, 451 (1961).
7. G.F. Gribakin, V.V. Flambaum, Phys. Rev. A **48**, 546 (1993).
8. M.J. Jamieson, A. Dalgarno, J. Phys. B **31**, L219 (1998).
9. J.R. Gardner, R.A. Cline, J.D. Miller, D.J. Heinzen, H.M.J.M. Boesten, B.J. Verhaar, Phys. Rev. Lett. **74**, 3764 (1995).
10. H.M.J.M. Boesten, C.C. Tsai, B.J. Verhaar, D.J. Heinzen, Phys. Rev. Lett. **77**, 5194 (1996).
11. E.R.I. Abraham, W.I. McAlexander, J.M. Gerton, R.G. Hulet, R. Côté, A. Dalgarno, Phys. Rev. A **53**, R3713 (1996).
12. E. Tiesinga, C.J. Williams, P.S. Julienne, K.M. Jones, P.D. Lett, W.D. Phillips, J. Res. Natl. Inst. Stand. Technol. **101**, 505 (1996).
13. A. Fioretti, D. Comparat, A. Crubellier, O. Dulieu, F. Masnou-Seeuws, P. Pillet, Phys. Rev. Lett. **80**, 4402 (1998).
14. E.R.I. Abraham, W.I. McAlexander, J.M. Gerton, R.G. Hulet, R. Côté, A. Dalgarno, Phys. Rev. A **55**, R3299 (1997).
15. C. C. Tsai, R. S. Freeland, J. M. Vogels , H. J. M. Boesten, B. J. Verhaar, D. J. Heinzen, Phys. Rev. Lett. **79**, 1245 (1997).
16. A.J. Moerdijk, B.J. Verhaar, Phys. Rev. Lett. **94**, 518 (1994).
17. R. Côté, A. Dalgarno, H. Wang, W.C. Stwalley, Phys. Rev. A **57**, R4118 (1998).
18. H. M. J. M. Boesten, C. C. Tsai, J. R. Gardner, D.J. Heinzen, B.J. Verhaar, Phys. Rev. A **55**, 636 (1997).
19. Ph. Courteille, R. S. Freeland, D.J. Heinzen, Phys. Rev. Lett. **81**, 69 (1998).
20. S. Inouye, M. R. Andrews, H.-J. Miesner, D. M. Stamper-Kurn, W. Ketterle, Nature **392**, 151 (1998).
21. J. P. Burke, C. H. Greene, J. L. Bohn, Phys. Rev. Lett. **81**, 3355 (1998).
22. M. J. Seaton, Rep. Prog. Phys. **46**, 167 (1983).
23. F. H. Mies, J. Chem. Phys. **80**, 2514 (1984).
24. W. E. Milne, Phys. Rev. **35**, 863 (1930).
25. H. J. Korsch, H. Laurent, J. Phys. B **14**, 4213 (1981).
26. M. Elbs, O. Keck, H. Knöckel, E. Tiemann, Z. Phys. D **42**, 49 (1997).
27. M. Elbs, H. Knöckel, T. Laue, Ch. Samuelis, E. Tiemann, to be published in Phys. Rev. A **59**, n. 5 (May 1999).
28. R.F. Barrows, J. Vergès, C. Effantin, K. Hussein, J. D'Incan, Chem. Phys. Lett. **104**, 179 (1984).
29. I. Velchev, R. van Dierendonck, W. Hogervorst, W. Ubachs, J. Mol. Spectr. **187**, 21 (1998).
30. K.M. Jones, S. Maleki, S. Bize, P.D. Lett,C.J. Williams, H. Richling, H. Knöckel, E. Tiemann, H. Wang, P.L. Gould, W.C. Stwalley, Phys. Rev. A **54**, R1006 (1996).
31. T.F. O'Malley, L. Spruch, L. Rosenberg, J. Math. Phys. **2**, 491 (1961).
32. G. N. Watson, "A Treatise on the theory of Bessel functions" (The University Press, Cambridge, 1966) chapt. 3.
33. P. Kharchenko, J.F. Babb, A. Dalgarno, Phys. Rev. A **55**, 3566 (1997).
34. F. Maeder, W. Kutzelnigg, Chem. Phys. **42**, 95 (1979).
35. D. Spelsberg, T. Lorenz, W. Meyer, J. Chem. Phys. **99**, 7845 (1993).
36. M. Marinescu, H.R. Sadeghpour, A. Dalgarno, Phys. Rev. A **49**, 982 (1994).
37. S.H. Patil, K.T. Tang, J. Chem. Phys. **106**, 2298 (1997).
38. C.R. Ekstrom, J. Schmiedmayer, M.S. Chapman, T.D. Hammond, D.E. Pritchard, Phys. Rev. A **51**, 3883 (1995).
39. G. Hadinger, G. Hadinger, S. Magnier, M. Aubert-Frecon, J. Mol. Spectrosc. **175**, 441 (1996).
40. A. Beckmann, K.D. Böklen, D. Elke, Z. Phys. **270**, 173 (1974).
41. E.R.I. Abraham, W.I. McAlexander, C.A. Sackett, R.G. Hulet, Phys. Rev. Lett. **74**, 1315 (1995).
42. C. Linton, T.L. Murphy, F. Martin, R. Bacis, J. Verges, J. Chem. Phys. **91** , 6036 (1995).